

New insight into effects of 4d transition metals doping on the photocatalytic activities of anatase TiO₂(101) surface

Yuehong Ren¹, Qingzhen Han², Qiaozhi Su¹, Jie Yang³, Yuehong Zhao⁴, Hao Wen⁴, and Zhaotan Jiang¹

¹Beijing Institute of Technology

²Beijing Academy of Quantum Information Sciences

³Shandong Graphenjoy Advanced Material CO. LTD

⁴Institute of Process Engineering Chinese Academy of Sciences

December 23, 2020

Abstract

Aiming at improving the visible-light photocatalytic activities of TiO₂(101) surface (TiOS) we make an in-dept study on the TiOS doped with 4d transition metal (TM) atoms. It is shown that the 4d TM dopings can not only produce new impurity energy bands in the bandgap but also result in the semiconductor-metal phase transition. Consequently, the visible-light absorption is strongly strengthened due to the dopings of Y, Zr, Nb, Mo, and Ag, while it is only weakly improved for Tc, Ru, Rh, Pd, and Cd dopings. The improvement in visible-light absorption can be attributed to the intraband or interband transition of electrons. Moreover, the photocatalytic activities are explored, and we find Y and Ag dopings can effectively enhance the photocatalytic activity of TiOS. Thus the mechanism of improving photocatalytic activity of TiOS has been clearly addressed, which is beneficial to further experimental and theoretical researches on TiO₂ photocatalysts.

1. Introduction

TiO₂, a promising semiconductor photocatalytic material, has attracted extensive attention due to its advantages, such as the biological and chemical inertness, stability to corrosion, nontoxicity, relatively low cost, and high photoactivity [1–3]. In nature, there exist three phases of TiO₂: rutile, anatase, and brookite TiO₂. Among them anatase TiO₂ is of the best photocatalytic activity and is widely applied in solar energy conversion, environmental purification, and particularly the degradation of harmful organic pollutants in water [4–6]. However, the popular application of anatase TiO₂ is severely restricted due to the following two reasons [7]: (i) The band gap E_g of 3.23 eV is so large that it leads to the low utilization efficiency of visible light; (ii) The quantum yield is very low because of the low electron transfer rate and the high recombination rate of photoexcited electron-hole pairs. Therefore, it is still urgent to improve the photocatalytic activity of TiO₂.

In the past decades, much effort has been devoted to extending the optical response range of TiO₂ to the visible-light region, by means of impurity doping [8–14], noble metal loading [15], semiconductor compounding [16–18], and organic sensitizing [19,20]. Among all these methods, impurity doping is considered to be one of the most convenient and efficient methods. In particular, transition metal (TM) atoms have been proven to be the ideal dopants to promote the photocatalytic performance of TiO₂ catalysts because of their d electronic configuration and unique characteristics. Quantum-sized TiO₂ doped with 0.5 at.% Fe³⁺, Mo⁵⁺, Ru³⁺, Os³⁺, Re⁵⁺, V⁴⁺, and Rh³⁺ are found to induce the red shift of absorption edge and can improve photoactivity for both CHCl₃ oxidation and CCl₄ reduction [21]. Mesoporous TiO₂ impregnated by Ag⁺, Co²⁺, Cu²⁺, Fe³⁺, and Ni²⁺ can accelerate the degradation of acetophenone and nitrobenzene in

aqueous solution [22]. TiO_2 powders doped by a small amount of Fe^{3+} can clearly enhance the intensity of absorption in the UV-visible light region and the photocatalytic oxidation of acetone in air [23]. Moreover, Ni 8 wt%-doped TiO_2 has a high photocatalytic activity for the decomposition of 4-chlorophenol in aqueous solution in the presence of both UV and visible light [24]. All the above researches have demonstrated that the TM dopants can extend the optical response range of TiO_2 into the visible-light region. However, we want to stress that the above dopings are mainly performed in bulk TiO_2 .

In fact, surface structure will play an important role in the photocatalytic activity because usually photocatalytic reactions mainly occur on the catalyst surface [25]. It is especially necessary to study the effect of the surface manipulation on the catalytic activity. Hebenstreit et al. [26] found that anatase $\text{TiO}_2(101)$ surface (TiOS) with few point defects is stable and the fourfold coordinated Ti atoms at step edges are the preferred adsorption sites. By investigating some low-index TiO_2 surfaces Labat et al. [27] demonstrated that the TiOS is the most stable surface. Also, Ma et al. [28] found that the TiOS structure with its outermost and second layers terminated by twofold coordinated O atoms and fivefold coordinated Ti atoms, respectively, is much more stable. Although many researches on the TiOS have been carried out, a systematic investigation on the photocatalytic activities of TiOS doped by all 4d TM atoms is still absent. A comparative study of all the 4d TM dopings on TiOS is required to clarify the intrinsic relation between the macroscopic photocatalytic activities and the microscopic TiO_2 details.

In this work, we will systematically investigate the surface modification of TiOS doped with 4d TM atoms to uncover how the doping will improve the photocatalytic performance of TiOS. We will first study the geometric structure, the doping manners, and the optical properties of the doped TiOS. Then, the relation of the macroscopic catalytic activity with the microscopic structure is discussed according to the density of states, energy bands, and the effective masses of carriers.

2. Computational methods

The geometric structure, the electronic structure, and the optical properties of the TiOS doped with ten 4d TM atoms Y, Zr, Nb, Mo, Tc, Ru, Rh, Pd, Ag, and Cd are calculated using the plane wave method based on the density functional theory (DFT). First, all the TiOS models doped in different doping manners are optimized, and the optimal doping manners of all TM atoms can be determined according to the impurity formation energy. Second, the band structures, the density of states, and the optical absorption coefficients of all the best doping models are calculated. All the calculations are performed with the Cambridge Serial Total Energy Package (CASTEP) [29]. The exchange-correlation potential is described by the Perdew-Burke-Ernzerhof (PBE) functional of the generalized gradient approximation (GGA) [30]. The cutoff energy for the plane wave basis set is set to be 340 eV. The Monkhorst-Pack scheme k-point grid sampling for the reduced Brillouin zone is set as $2 \times 4 \times 1$, and the convergence criteria for the self-consistent field (SCF) is set to 1.0×10^{-6} eV/atom. All the atom coordinates are fully optimized until the forces on every atom are smaller than 0.03 eV/Å. The interaction between the valence electrons and the ionic core is described by the ultrasoft pseudopotential [31].

The formation energy is defined as

$$E_f(M) = \frac{E(M\text{-TiO}_2) - E(\text{TiO}_2) - E(M)}{48}, \quad (1)$$

where $E(M)$ is the energy of an isolated TM atom, and $E(\text{TiO}_2)$ [$E(M\text{-TiO}_2)$] is the total energy of the pure [TM-atom-doped] TiOS. For convenience, all of the optimal doping models can be denoted as $\text{Ti}_{24}\text{M}\text{O}_{48}$ with M representing the TM atoms Y, Zr, Nb, Mo, Tc, Ru, Rh, Pd, Ag, and Cd.

As widely recognized, the transfer rate of charge carriers can play a vital role in determining the photoactivity of a semiconductor material [32,33], and can be defined as [32,34]

$$v = \hbar k / m^*, \quad (2)$$

where \hbar is the reduced Planck constant, k is the wave vector, and m^* is the effective mass of charge carrier. The effective masses of electrons (m_e^*) and holes (m_h^*) can be obtained by fitting the energy band around

the valence band maximum (VBM) and the conduction band minimum (CBM) along a specific direction in the reciprocal space, respectively. It should be noticed that the region used for parabolic fitting is kept in a very small interval to ensure the validity of the parabolic approximation. In addition, to clarify the difference between the effective masses of electrons and holes, an effective mass ratio r_{he} is introduced as

$$r_{he} = \frac{m_h^*}{m_e^*}. \quad (3)$$

In general, a larger r_{he} value indicates $m_h^* > m_e^*$, resulting in a larger difference of the carrier velocities and a slower recombination rate of the photogenerated electron-hole pairs [32].

3. Results

3.1. Optimal doping manners

Fig. 1 shows the anatase TiO_2 unit cell in which there exist four titanium atoms and eight oxygen atoms. The lattice parameters a , c , d_{eq} , d_{ap} , c/a , u ($=d_{ap}/c$), 2θ , and the unit cell volume V_0 (see Fig. 1a) are listed in Table 1 so as to compare with the experimental values [35] and other theoretical results [36]. Clearly, the lattice parameters obtained in this work are in better agreement with the experimental data than other theoretical values, demonstrating the reliability of the calculation method and the models adopted here.

Fig. 1 (Color online) (a) The optimized unit cell of anatase TiO_2 . (b) Different doping manners on TiOS.

Table 1 Optimized lattice parameters of the anatase TiO_2 unit cell in comparison with experimental and theoretical results.

Lattice parameters	Exp.[35]	This work	Theo.[36]
a (Å)	3.782	3.743	3.692
c (Å)	9.502	9.483	9.471
d_{eq} (Å)	1.932	1.914	1.893
d_{ap} (Å)	1.979	1.970	1.948
c/a	2.512	2.534	2.566
u	0.208	0.208	0.206
2θ (°)	156.3	155.8	154.4
V_0 (Å ³ /TiO ₂)	33.98	33.21	32.27

Starting from the optimized anatase TiO_2 unit cell, we construct the TiOS model with the outermost and second layers terminated by twofold coordinated O atoms and fivefold coordinated Ti atoms, respectively. The doping concentration of TiOS doped with TM atoms is 1.37 at.% and six typical doping manners in Fig. 1b are considered. A TM atom can be vertically adsorbed on a twofold coordinated O atom (O1-Ad), threefold coordinated O atoms (O2-Ad, O3-Ad), a fivefold coordinated Ti atom (Ti1-Ad), and a sixfold coordinated Ti atom (Ti2-Ad). In addition, TM atoms are only allowed to enter the largest and outermost caves (Cav) because of their large atomic radii. Table 2 shows the impurity formation energies E_f for ten different 4d TM atom doped models of the TiOS in six different doping manners. We can see only Ag-Cav and Cd-Cav dopings have positive E_f , indicating these two doping processes correspond to endothermic reactions, and are difficult to occur. This should be reasonable since the structures with Ag or Cd atoms doped into the caves are unstable owing to the large atom radii of Ag and Cd. However, all the other doped cases studied here have negative E_f , which indicates the corresponding doping processes are exothermic reactions that can occur more easily. Furthermore, the optimal doping manners for all TM atoms can be readily found according to the lowest E_f , and listed in the following: O1-Ad doping for Ru, O2-Ad doping for Pd and Ag, O3-Ad doping for Y and Rh, Ti1-Ad doping for Tc and Cd, and Cav doping for Zr, Nb, and Mo. Obviously, different TM atoms have different optimal doping manners. In fact, even in the same doping

manner, the impurity atoms may have various positions after being optimized. In particular, Tc, Pd, Ag, and Cd atoms, having stable full or half-full filling outermost orbitals, prefer the O2-Ad or Ti1-Ad doping, while Y, Zr, Nb, Mo, and Rh atoms with unstable outermost orbitals and spin multiplicity, prefer the O3-Ad or Cav doping. The different optimal doping manners are closely dependent on the 4d electron configuration, the atomic radius, and the electronegativity of the TM atom. Thus, the optimal doping manners of all 4d TM atoms have been determined.

Table 2 The formation energies (eV) of TiOS doped with 4d TM atoms.

	O1-Ad	O2-Ad	O3-Ad	Ti1-Ad	Ti2-Ad	Cav
Y(4d ¹ 5s ²)	-3.992	-3.991	-3.996	-3.991	-3.995	-2.780
Zr(4d ² 5s ²)	-6.238	-6.544	-6.187	-6.245	-5.684	-7.045
Nb(4d ⁴ 5s ¹)	-4.727	-4.725	-4.715	-4.726	-3.377	-4.888
Mo(4d ⁵ 5s ¹)	-2.502	-2.394	-2.972	-2.396	-2.454	-2.989
Tc(4d ⁵ 5s ²)	-3.447	-3.448	-3.227	-3.449	-2.242	-3.314
Ru(4d ⁷ 5s ¹)	-3.341	-3.339	-3.338	-3.340	-2.354	-2.554
Rh(4d ⁸ 5s ¹)	-0.8964	-1.128	-1.364	-0.8950	-1.130	-0.2150
Pd(4d ¹⁰)	-1.381	-1.484	-1.434	-1.379	-1.483	-1.014
Ag(4d ¹⁰ 5s ¹)	-0.5412	-0.9686	-0.9660	-0.5548	-0.5511	0.4253
Cd(4d ¹⁰ 5s ²)	-0.0847	-0.0953	-0.1657	-0.1661	-0.1035	2.376

3.2. Optical absorption

Now we study the optical absorption properties of TiOS doped with 4d TM atoms, as shown in Fig. 2. For comparison, the optical absorption properties of the pure TiOS are also plotted by the dash-dotted curves. The scissor operator, namely, the difference 1.03 eV between the experimental band gap (3.23 eV) and the calculated band gap (2.20 eV) is applied to correct the optical properties [32]. For the pure TiOS, the absorption edge is located at around 392 nm as shown in Fig. 2, in agreement with the experimental observation [37] and the theoretical result [38]. This indicates that the optical response is mainly localized in the UV-light region, inducing that the utilization ratio of visible light (approximately 380–780 nm) will be quite low. Therefore, it is necessary to modify the physicochemical properties of TiOS to achieve a better visible-light response. By comparing the solid curve with the dash-dotted one in each pannel in Fig. 2, we can find all 4d TM atoms are able to improve the visible-light response of TiOS to different degrees. Totally speaking, their optical absorption coefficients can be classified into two types: (1) Strong improvement case. In Figs. 2a-2e, we can find that high and wide absorption peaks can be formed in the visible-light region, clearly indicating that the visible-light absorption coefficients are significantly increased for Ti₂₄YO₄₈, Ti₂₄ZrO₄₈, Ti₂₄NbO₄₈, Ti₂₄MoO₄₈, and Ti₂₄AgO₄₈. Notably, the Nb doped TiOS shows the best visible-light response. These results imply that the 4d TM dopants with a half-full or less than half-full outer electron configuration can obviously improve the visible-light response of TiOS. (2) Weak improvement case. In Figs. 2f-2j, the visible-light absorption coefficients are only slightly increased for Ti₂₄TcO₄₈, Ti₂₄RuO₄₈, Ti₂₄RhO₄₈, Ti₂₄PdO₄₈, and Ti₂₄CdO₄₈, implying there exists a weak improvement in the visible-light response. Moreover, we can find that the visible-light response intensity will decrease as the atomic number of the dopants increases from Y, Zr, Nb, Mo to Tc, or from Ru, Rh, Pd to Cd. Yet, very surprisingly, Ag with a large atomic number will show unexpected strong visible-light response, different from its neighboring elements. Furthermore, we can find that the 4d TM atom doping induced absorption improvement can appear in a wide area with the wavelength much longer than the visible-light wavelength. This phenomenon is especially outstanding for the strong improvement case in relative to the weak improvement one. Therefore, we can conclude that, among the investigated 4d TM dopings, the TiOS doped with Y, Zr, Nb, Mo, and Ag can remarkably improve the utilization efficiency of visible light.

Fig. 2 (Color online) The optical absorption coefficients of pure (dash-dotted curve) and doped (solid curve) TiOS. The region between two vertical dotted lines represent the visible-light region.

3.3. Density of states

In order to clearly understand the optical absorption properties, Fig. 3 shows the total density of states (TDOS) and partial density of states (PDOS) near the Fermi level of pure and 4d TM atom doped TiOS with spin-up (spin-down) states plotted on the positive (negative) y-axes. In view of the presence of unpaired electrons, it is necessary to take spin into account for the dopings of Y, Zr, Nb, Mo, Tc, Ru, and Rh atoms, while it is not for the dopings of Pd, Ag, and Cd atoms. For the pure TiOS, as shown in Fig. 3a, both the valence band (VB) and the conduction band (CB) are formed by the mixing of O 2p and Ti 3d states. However, the VB is mainly contributed by O 2p states, while the CB is mainly contributed by Ti 3d states. This composition of the VB and CB will not be qualitatively changed by the dopings of 4d TM atoms. However, both VB and CB of all the doped TiOS are seriously shifted to the low energy region in comparison with those of pure TiOS, which should stem from the upward shift of the Fermi energy level. For the dopings of Y, Zr, Nb, Mo, and Ag atoms, the Fermi energy levels move into the CB as shown in Figs. 3b-3f, and they can be viewed as n-type conductors. So we think the dopings can induce the semiconductor-metal phase transition. Therefore, lower energy photons can be absorbed by electron to induce the intra-band transition. Thus, the light absorption response in the entire visible light region or even longer wavelength range may be strengthened, which clearly explains the increase of the optical absorption in Figs. 2a-2e. However, the Fermi energy levels for the dopings of Tc, Ru, Rh, Pd, and Cd atoms seem to stay in the original band gaps in Figs. 3g-3k, implying that only the inter-band transition can occur, sharply different from those of the dopings of Y, Zr, Nb, Mo, and Ag atoms in Figs. 3b-3f. By a close look at Figs. 3g-3k, we can see that the new bands are formed by the coupling of the 4d states of the TM atoms and the O 2p or Ti 3d states. Obviously, this kind of inter-band transition will contribute to the visible-light absorption. Intuitively and reasonably, the relatively small amount of dopants will induce relatively weak light absorption. This is the reason why only the weak improvement can appear in Figs. 2g-2k. Although the doping-induced new bands can also be observed for Y, Zr, Nb, and Mo in Figs. 3b-3e, the Fermi level is deeply immersed into the original CB. In this case it is the intra-band transition in the original CB that dominates the light absorption, which induces the appearing of the strong improvement of the visible-light absorption.

Fig. 3 (Color online) The TDOS and PDOS of pure and 4d TM doped TiOS. For clarity, the Fermi energy level is shown by the vertical dotted lines at zero energy.

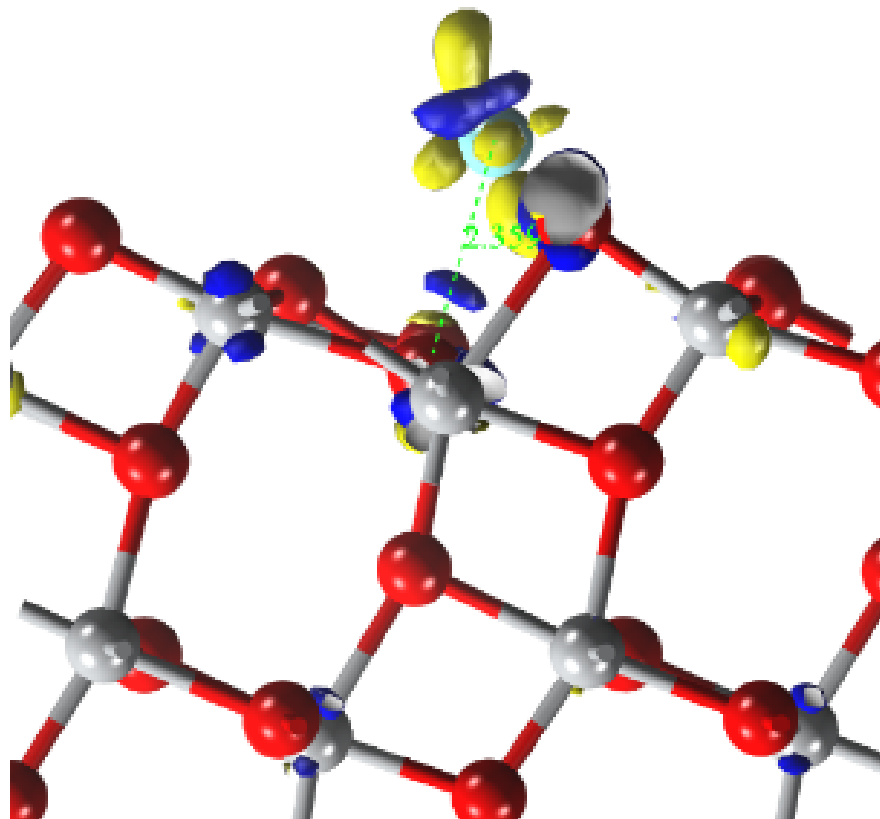
3.4. Band structure

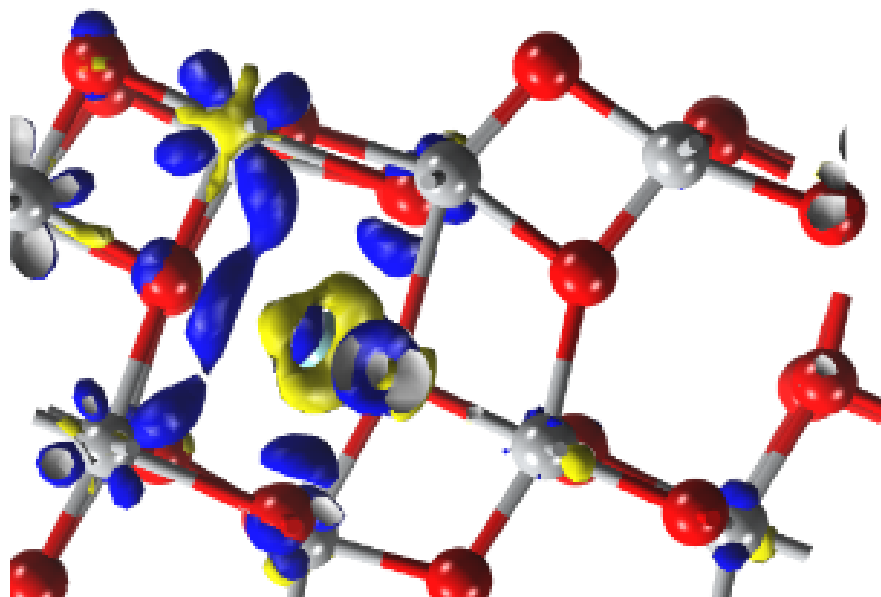
In order to explain more intuitively the optical absorption, we further show the energy bands of the 4d TMs doped TiOS in Fig. 4. For pure TiOS in Fig. 4a, the VBM and the CBM are located at G point, indicating the nature of the direct band gap. For 4d TM doped TiOS, the VBM and CBM are still located at G point. However, most of dopings except Ag will introduce the impurity energy levels (IELs) in the band gap of pure TiOS. As shown in Figs. 4b-4e, the IELs of $\text{Ti}_{24}\text{YO}_{48}$, $\text{Ti}_{24}\text{ZrO}_{48}$, $\text{Ti}_{24}\text{NbO}_{48}$, and $\text{Ti}_{24}\text{MoO}_{48}$ are located slightly below the CBM, which can reduce the energy required for the electron transition to the CB and be beneficial for extending the light absorption to visible region and eventually enhancing the visible-light absorption efficiency. Besides, the Fermi energy levels of $\text{Ti}_{24}\text{YO}_{48}$, $\text{Ti}_{24}\text{ZrO}_{48}$, $\text{Ti}_{24}\text{NbO}_{48}$, $\text{Ti}_{24}\text{MoO}_{48}$, and $\text{Ti}_{24}\text{AgO}_{48}$ enter the CB in Figs. 4b-4f, resulting in the intra-band transition, which effectively induces stronger light absorption. For the weak improvement case, the IELs of $\text{Ti}_{24}\text{TcO}_{48}$ and $\text{Ti}_{24}\text{RuO}_{48}$ in Figs. 4g and 4h are located near CBM, while the IELs of $\text{Ti}_{24}\text{RhO}_{48}$ and $\text{Ti}_{24}\text{PdO}_{48}$ in Figs. 4i and 4j are located near VBM. In the same way, the existence of IELs can reduce the energy required for the electron transition, and hence enhance the optical absorption in the visible-light region.

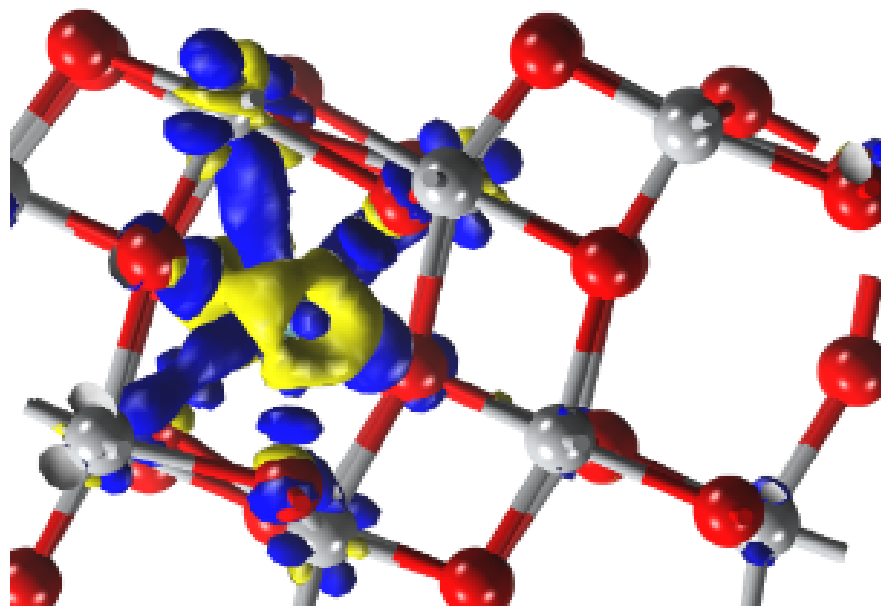
Fig. 4 (Color online) The band structure of pure and 4d TM doped TiOS. In (b, c, d, e, g, h, i) the solid (dotted) curve represents the spin-up (spin-down) state. The horizontal dashed lines at the energy zero represent the Fermi energy levels.

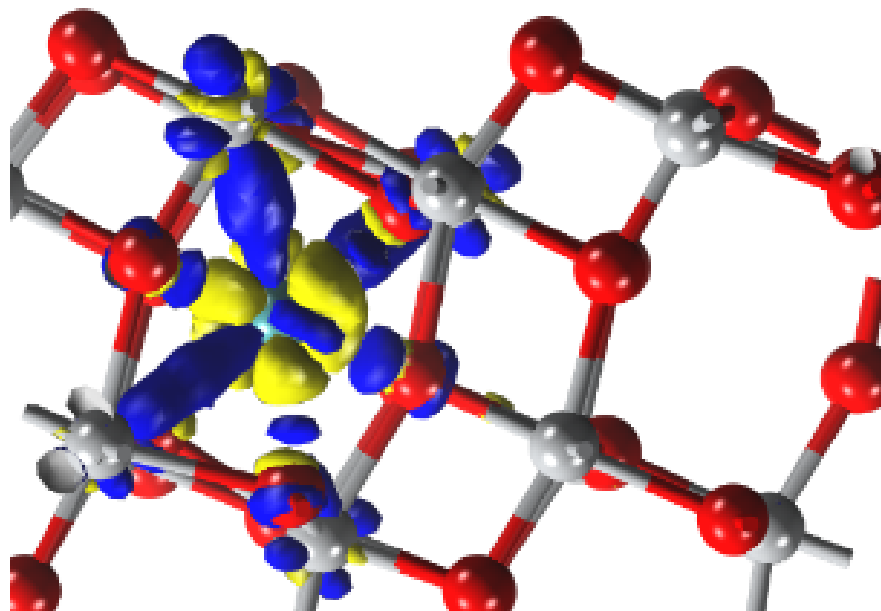
Next, in Fig. 5 we present the Mulliken charge of the 4d TM doped TiOS. From Fig. 5a we can see that all 4d TM atoms will carry positive charges and there exist equivalent negative charges appearing in TiOS, indicating the electron transferring from 4d TM atoms to TiOS. Clearly Y, Zr, Nb and Mo can carry

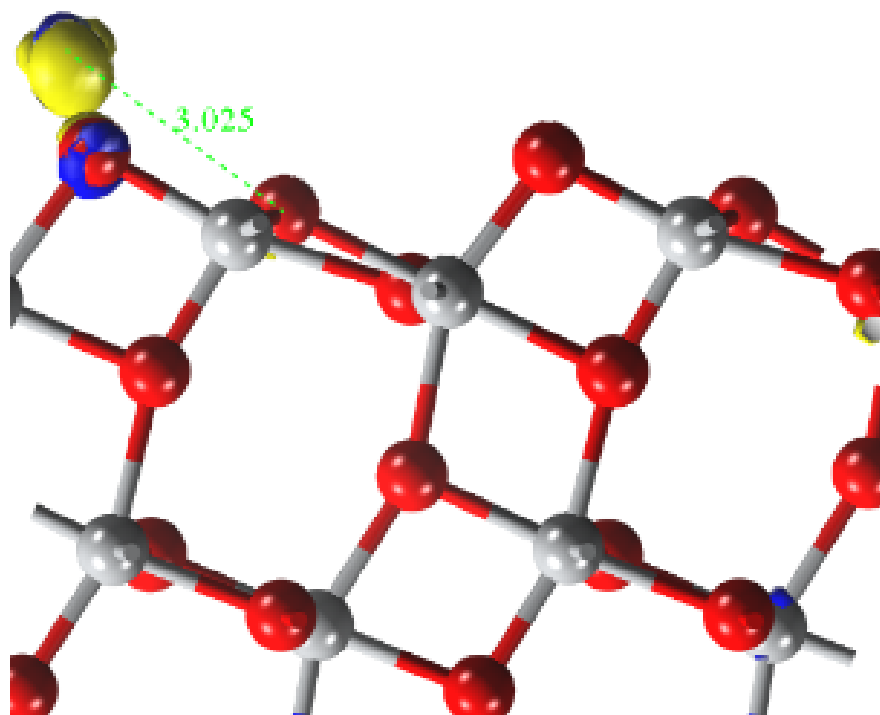
much more positive charges than Ru, Rh, Pd and Cd. Large positive charges on doping atoms indicate more electrons on the doping atoms will move from doping atoms to TiOS, further leading to the positive charge centers and making the original CB are filled by electrons. This clearly expounds why the Fermi energy levels are shifted into the CB. Small positive charges on the doping atoms may indicate the electric polarization of the doping atoms and their surroundings. In this case no obvious electron transfer will occur. Also, we present in Fig. 5b-5k the charge density differences of all doped models which vividly depict the redistribution of the electrons in the 4d TM doped TiOS.

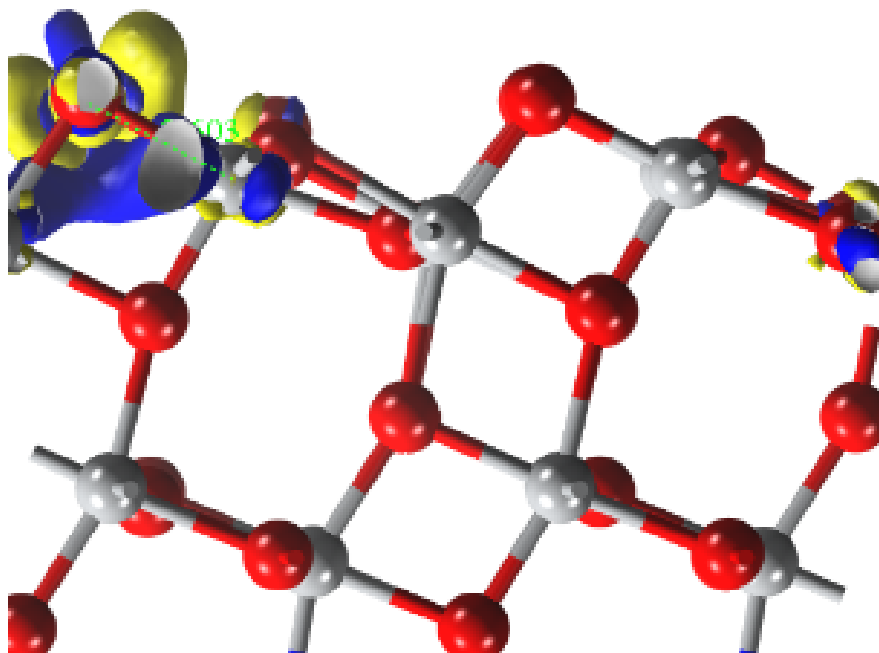


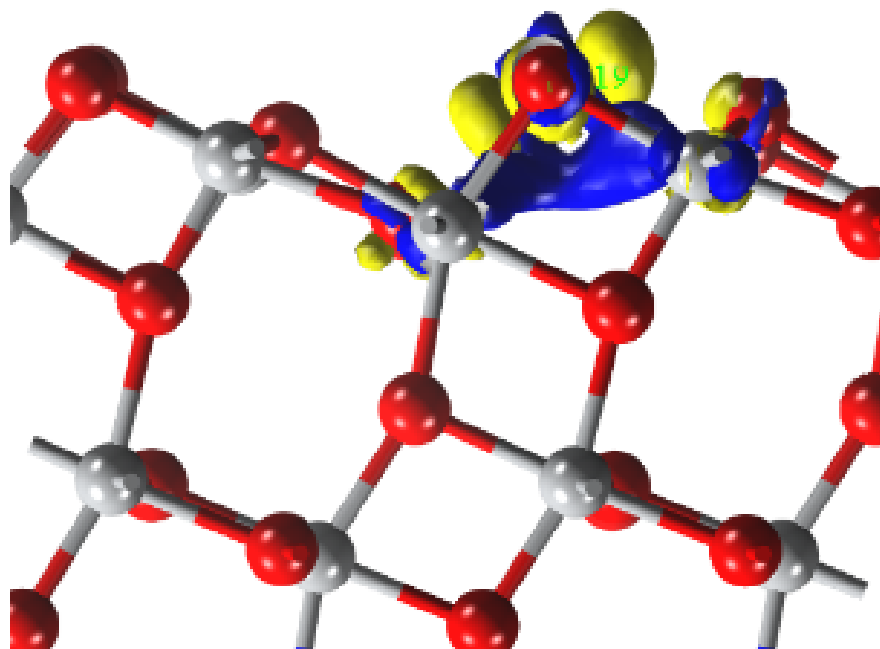


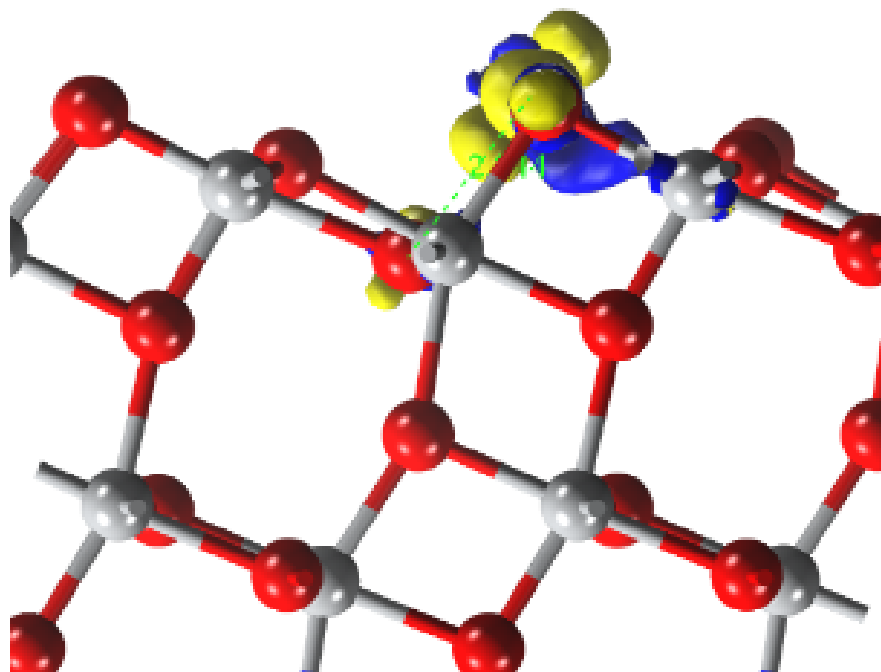


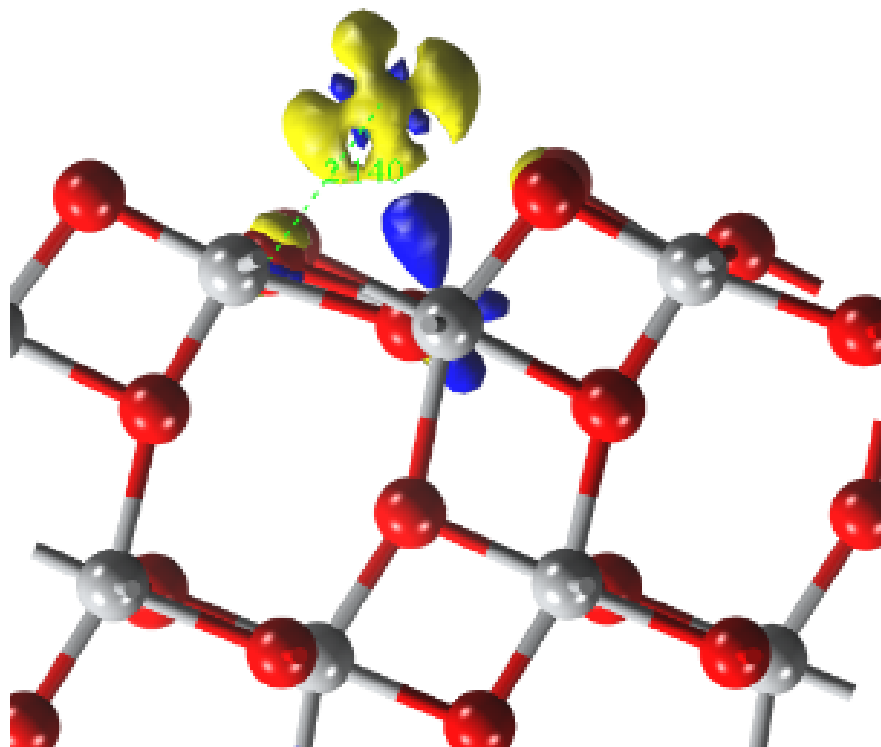












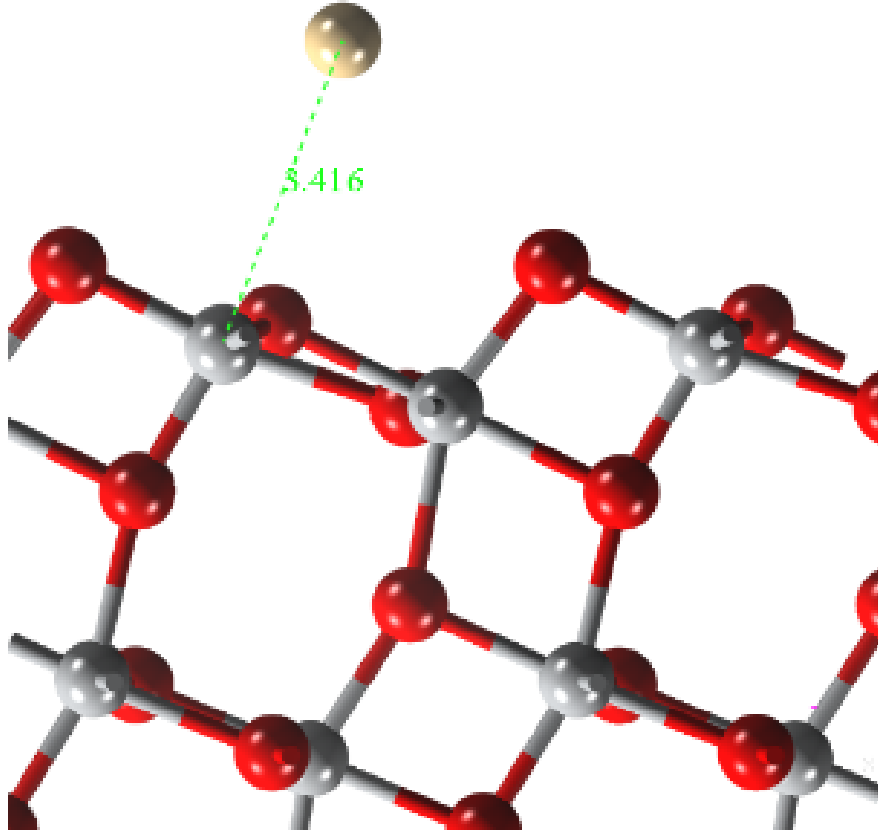


Fig. 5 (Color online) (a) Mulliken charge distribution of 4d TM atoms in doped models. (b-k) Charge density difference in 4d TMs doped TiOS with an isovalue of $0.06 \text{ e}/\text{\AA}^3$. Blue (dark) and yellow (grey) areas represent electron accumulation and depletion, respectively.

3.6. Photocatalytic activities

In order to analyze the effect of the 4d TM atom doping on the photocatalytic activity of TiOS, we resort to the effective masses and the transfer rates of the photogenerated electrons and holes. For the pure TiOS, the effective masses are found to be $m_h^*(p) = 17.348m_0$ and $m_e^*(p) = 2.387m_0$ with m_0 being the electron mass, which implies a large $r_{he}(p) = 7.268$. This large difference between $m_h^*(p)$ and $m_e^*(p)$ will further result in the large difference between the transfer rates of electrons and holes, reducing the recombination of electrons and holes. Therefore, TiOS can be used as a promising photocatalytic material. When TiOS is doped by 4d TM atoms, the effective masses of electrons and holes are denoted by $m_h^*(d)$ and $m_e^*(d)$ along one certain direction, respectively. We can see in Fig. 6 that the relative variation ratios $r_h = m_h^*(d)/m_h^*(p)$ are all greater than 1, indicating the doping can seriously increase the effective mass of the photogenerated holes. However, the relative variation ratios $r_e = m_e^*(d)/m_e^*(p)$ are all close to 1, indicating only tiny variations of m_e^* are observed. Therefore the doping will make stronger influences on the effective mass of the holes than the electrons. For clarity, we also plot the ratio $r'_{he} = r_{he}(d)/r_{he}(p)$ to clearly reflect the overall doping induced variations of the hole and electron effective masses with $r_{he}(d)$ and $r_{he}(p)$ being the effective mass ratios corresponding to the doped and pure TiOS. We can see all r'_{he} are greater than 1, indicating all the dopings can enlarge the effective mass difference between holes and electrons. This phenomenon is more evident for Y, Zr, Nb, Mo, and Ag than Tc, Ru, Rh, Pd, and Cd. Furthermore, this demonstrates that the 4d TM atom doping will further suppress the recombination of the photogenerated electrons and holes, which can improve the photocatalytic activity of TiOS in different degrees. Moreover, the dopings of Y and

Ag can lead to larger r'_{he} , indicating both Y and Ag dopings can be viewed as the better schemes used to enhance photocatalytic activity of TiOS.

Fig. 6 (Color online) The relative variation ratios r_h , r_e , and r'_{he} for different doping models.

Furthermore, as discussed before, based on the energy bands of the 4d TM atom doped TiOS in Fig. 4 we can see that the couplings of the doping atoms and the TiOS can produce new impurity energy bands in the original band gap and fill the original CB with electrons. The appearing of the impurity energy bands will provide new channels through which the electrons in impurity bands can be pumped to the CB by absorbing the visible-light photons. Therefore, this procedure can strengthen the visible-light induced photocatalytic activities of TiOS. Moreover, the visible-light absorption will also pump the electron below Fermi energy level in the CB into the empty energy levels above Fermi energy level, inducing more electron to appear at high energy levels. This also increases the photocatalytic activities of the TiOS. Thus we can draw that the 4d TM atom dopings are beneficial for increasing the visible-light utilization efficiency and improving the photocatalytic activities of TiOS.

4. Conclusion

In summary, we have systematically studied the TiOS doped by all 4d TM atoms. New impurity energy bands can be generated in the bandgap and the semiconductor-metal phase transition can be induced by dopings. The visible-light absorption can be seriously increased by doping Y, Zr, Nb, Mo, and Ag, and only weakly increased by doping other 4d TM atoms. The former should be caused by both interband and intraband transitions of electrons while the latter should be only the interband transition. Furthermore, we discussed the doping-induced improvement of the photocatalytic activities of TiOS. It is verified that among all 4d TM atoms both Y and Ag dopings can be used to effectively improve the visible-light photocatalytic activities of the TiOS.

Acknowledgements

The authors gratefully acknowledge the financial support from the National Natural Science Foundation of China (No. 11774029) and the CAS Informatization Program of the Thirteenth Five-Year Plan (No. XXH1350303-103).

References

1. Etacheri, V.; Di Valentin, C.; Schneider, J.; Bahnemann, D.; Pillai, S. C. Visible-light activation of TiO₂ photocatalysts: Advances in theory and experiments. *J. Photochem. Photobiol. C* 2015, 25, 1–29.
2. Khaki, M. R. D.; Shafeeyan, M. S.; Raman, A. A. A.; Daud, W. M. A. Application of doped photocatalysts for organic pollutant degradation—a review. *J. Environ. Manage.* 2017, 198, 78–94.
3. Mazierski, P.; Mikolajczyk, A.; Bajorowicz, B.; Malankowska, A.; Zaleska-Medynska, A.; Nadolna, J. The role of lanthanides in TiO₂-based photocatalysis: a review. *Appl. Catal. B* 2018, 233, 301–317.
4. Chen, D.; Cheng, Y.; Zhou, N.; Chen, P.; Wang, Y.; Li, K.; Huo, S.; Cheng, P.; Peng, P.; Zhang, R.; Wang, L.; Liu, H.; Liu, Y.; Ruan, R. Photocatalytic degradation of organic pollutants using TiO₂-based photocatalysts: a review. *J. Cleaner Prod.* 2020, 268, 121725.
5. Diebold, U. The surface science of titanium dioxide. *Surf. Sci. Rep.* 2003, 48, 53–229.
6. Kumaravel V.; Mathew, S.; Bartlett, J.; Pillai, S. C. Photocatalytic hydrogen production using metal doped TiO₂: a review of recent advances. *Appl. Catal. B* 2019, 244, 1021–1064.
7. Li, X. Z.; Li, F. B.; Yang, C. L.; Ge, W. K. Photocatalytic activity of WO_x-TiO₂ under visible light irradiation. *J. Photochem. Photobiol. A* 2001, 141, 209–217.
8. Asahi, R.; Morikawa, T.; Ohwaki, T.; Aoki, K.; Taga, Y. Visible-light photocatalysis in nitrogen-doped titanium oxides. *Science* 2001, 293, 269–271.
9. Chen, X.; Burda, C. The electronic origin of the visible-light absorption properties of C-, N- and S-doped TiO₂ nanomaterials. *J. Am. Chem. Soc.* 2008, 130, 5018–5019.
10. Li, Z.; Shen, W.; He, W.; Zu, X. Effect of Fe-doped TiO₂ nanoparticle derived from modified hydrothermal process on the photocatalytic degradation performance on methylene blue. *J. Hazard. Mater.*

- 2008, 155, 590–594.
11. Ganesh, I.; Gupta, A. K.; Kumar, P. P.; Sekhar, P. S. C.; Radha, K.; Padmanabham. G.; Sundararajan, G. Preparation and characterization of Ni-doped TiO₂ materials for photocurrent and photocatalytic applications. *Sci. World J.* 2012, 2012, 127326.
 12. Sakatani, Y.; Ando, H.; Okusako, K.; Koike, H.; Nunoshige, J.; Takata, T.; Kondo, J. N.; Hara, M.; Domen, K. Metal ion and N co-doped TiO₂ as a visible-light photocatalyst. *J. Mater. Res.* 2004, 19, 2100–2108.
 13. Xing, M.; Wu, Y.; Zhang, J.; Chen, F. Effect of synergy on the visible light activity of B, N and Fe co-doped TiO₂ for the degradation of MO. *Nanoscale* 2010, 2, 1233–1239.
 14. Khan, M.; Gul, S. R.; Li, J.; Cao, W. Photocatalytic degradation of methylene blue by hydrothermally prepared Ag-doped TiO₂ under visible light irradiations. *JOM* 2015, 67, 2104–2107.
 15. Anpo, M.; Takeuchi, M. The design and development of highly reactive titanium oxide photocatalysts operating under visible light irradiation. *J. Catal.* 2003, 216, 505–516.
 16. Fujii, H.; Inata, K.; Ohtaki, M.; Eguchi, K.; Arai, H. Synthesis of TiO₂/CdS nanocomposite via TiO₂ coating on CdS nanoparticles by compartmentalized hydrolysis of Ti alkoxide. *J. Mater. Sci.* 2001, 36, 527–532.
 17. Ismail, A. A.; Lars, R.; Bahnemann, D. W. Study of the efficiency of UV and visible-light photocatalytic oxidation of methanol on mesoporous RuO₂-TiO₂ nanocomposites. *Chem. Phys. Chem.* 2011, 12, 982–991.
 18. Chainarong, S.; Niyomwas, S.; Sikong, L.; Pavasupree, S. The effect of molar ratio of TiO₂/WO₃ nanocomposites on visible light prepared by hydrothermal method. *Adv. Mater. Res.* 2012, 488–489, 572–577.
 19. Hahlin, M.; Johansson, E. M. J.; Plogmaker, S.; Odelius, M.; Hagberg, D. P.; Sun, L.; Siegbahn, H.; Rensmo, H. Electronic and molecular structures of organic dye/TiO₂ interfaces for solar cell applications: a core level photoelectron spectroscopy study. *Phys. Chem. Chem. Phys.* 2010, 12, 1507–1517.
 20. Nishikawa, M.; Sakamoto, H.; Nosaka, Y. Reinvestigation of the photocatalytic reaction mechanism for Pt-complex-modified TiO₂ under visible light irradiation by means of ESR spectroscopy and chemiluminescence photometry. *J. Phys. Chem. A* 2012, 116, 9674–9679.
 21. Choi, W.; Termin, A.; Hoffmann, M. R. The role of metal ion dopants in quantum-sized TiO₂: correlation between photoreactivity and charge carrier recombination dynamics. *J. Phys. Chem.* 1994, 98, 13669–13679.
 22. Tayade, R. J.; Kulkarni, R. G.; Jasra, R. V. Enhanced photocatalytic activity of TiO₂-coated NaY and HY zeolites for the degradation of methylene blue in water. *Ind. Eng. Chem. Res.* 2007, 46, 369–376.
 23. Zhou, M.; Yu, J.; Cheng, B. Effects of Fe-doping on the photocatalytic activity of mesoporous TiO₂ powders prepared by an ultrasonic method. *J. Hazard. Mater.* 2006, 137, 1838–1847.
 24. Kim, D. H.; Lee, K. S.; Kim, Y. S.; Chung, Y. C.; Kim, S. J. Photocatalytic activity of Ni 8 wt%-doped TiO₂ photocatalyst synthesized by mechanical alloying under visible light. *J. Am. Ceram. Soc.* 2006, 89, 515–518.
 25. Jia, C.; Fan, W.; Yang, F.; Zhao, X.; Sun, H.; Li, P.; Liu, L. A theoretical study of water adsorption and decomposition on low-index spinel ZnGa₂O₄ surfaces: correlation between surface structure and photocatalytic properties. *Langmuir* 2013, 29, 7025–7037.
 26. Hebenstreit, W.; Ruzycki, N.; Herman, G. S.; Gao, Y.; Diebold, U. Scanning tunneling microscopy investigation of the TiO₂ anatase (101) surface. *Phys. Rev. B* 2000, 62, R16334–R16336.
 27. Labat, F.; Baranek, P.; Adamo, C. Structural and electronic properties of selected rutile and anatase TiO₂ surfaces: An ab initio investigation. *J. Chem. Theory Comput.* 2008, 4, 341–352.
 28. Ma, X. G.; Tang, C. Q.; Huang, J. Q.; Hu, L. F.; Xue, X.; Zhou, W. B. First-principle calculations on the geometry and relaxation structure of anatase TiO₂ (101) surface. *Chinese J. Phys.* 2006, 55, 4208–4213.
 29. Segall, M. D.; Lindan, P. J. D.; Probert, M. J.; Pickard, C. J.; Hasnip, P. J.; Clark, S. J.; Payne, M. C. First-principles simulation: ideas, illustrations and the CASTEP code. *J. Phys.: Condens. Matter* 2002, 14, 2717–2744.

30. Perdew, J. P. Burke, K. Ernzerhof, M. Generalized gradient approximation made simple, *Phys. Rev. Lett.* 1996, 77, 3865–3868.
31. Vanderbilt, D. Soft self-consistent pseudopotentials in a generalized eigenvalue formalism, *Phys. Rev. B* 1990, 41, 7892–7895.
32. Yu, W.; Zhang, J.; Peng, T. New insight into the enhanced photocatalytic activity of N-, C- and S-doped ZnO photocatalysts. *Appl. Catal. B* 2016, 181, 220–227.
33. Etacheri, V.; Di Valentin, C.; Schneider, J.; Bahnemann, D.; Pillai, S.C. Visible-light activation of TiO₂ photocatalysts: advances in theory and experiments. *J. Photochem.* 2015, 25, 1–29.
34. Yu, J.; Zhou, P.; Li, Q. New insight into the enhanced visible-light photocatalytic activities of B-, C- and B/C-doped anatase TiO₂ by first-principles. *Phys. Chem. Chem. Phys.* 2013, 15, 12040–12047.
35. Burdett, J. K.; Hughbanks, T.; Miller, G. J.; Richardson, J. W.; Smith, J. V. Structural-electronic relationships in inorganic solids: powder neutron diffraction studies of the rutile and anatase polymorphs of titanium dioxide at 15 and 295 K. *J. Am. Chem. Soc.* 1987, 109, 3639–3646.
36. Asahi, R.; Taga, Y.; Mannstadt, W.; Freeman, A. J. Electronic and optical properties of anatase TiO₂. *Phys. Rev. B* 2000, 61, 7459–7465.
37. Boschloo, G. K.; Goossens, A.; Schoonman, J. Photoelectrochemical study of thin anatase TiO₂ films prepared by metallorganic chemical vapor deposition. *J. Electrochem. Soc.* 1997, 144, 1311–1317.
38. Yang, Y.; Feng, Q.; Wang, W.; Wang, Y. First-principle study on the electronic and optical properties of the anatase TiO₂(101) surface. *J. Semicond.* 2013, 34, 073004-1–073004-5.